**ONLINE FIRST June 8, 2026**

*Engineering Transactions*, **74**, https://doi.org/10.24423/engtrans.2026.3641
Institute of Fundamental Technological Research Polish Academy of Sciences (IPPT PAN)
Université de Lorraine • Poznan University of Technology

## Research Paper

# Global Buckling of a Thin-Walled T-Frame with Consideration of the Shear Effect

Krzysztof Magnucki[1)], Paweł Jasion[2)*]

[1)] *Łukasiewicz Research Network – Poznan Institute of Technology*
Poznań, Poland

[2)] *Institute of Applied Mechanics, Poznan University of Technology*
Poznań, Poland

*Corresponding Author: pawel.jasion@put.poznan.pl

This work concerns a global elastic buckling problem of a thin-walled T-frame with consideration of the shear effect. A novel approach was used to account for this effect, namely, the non-linear shear deformation theory, which gives as a result the shear deformation function describing the behaviour of the beam cross section. This thin-walled T-frame consists of a horizontal beam and a vertical column made of the same standard H-beams. The shape of this standard H-beam and the dimensionless deformation function of the plane cross section, being the result of the shear effect, are analytically described. The buckling problem of the frame is analytically formulated and solved. The critical loads of exemplary beams are analytically determined. Moreover, a numerical model, based on the finite element method (FEM), of the frame is elaborated and the critical loads of exemplary frames are determined. Consequently, the research results obtained by both methods are compared, and the advantages of the proposed approach are discussed.

**Keywords:** elastic buckling, frame, H-beam, thin-walled beam, shear effect.



## 1. Introduction

Thin-walled beams used in the 20th century are still commonly used today, for example, in vehicles and steel building structures. They are parts of frames containing from several to several dozen beams. Particular beams may be subjected to different types of loading such as compression, torsion or bending; however usually a complex state of stress in each beam is present. For this reason, an effective tool is needed to analyse the state of stress in the beam, the phenomena occurring at the joints between beams as well as the influence of individual beams on each other. A detailed description of the strength and

stability problems of thin-walled beams and selected structures is provided by TRAHAIR *et al.* [1]. The authors described in detail problems related to tension and compression members, local buckling of thin-plate elements, bending and lateral buckling of beams, beam-columns, frames, joints, and torsion members.

The application of the generalised beam theory (GBT) to the analysis of thin-walled frames is presented by BASAGLIA *et al.* [2]. The buckling analysis of frames made of U- and I-sections is discussed, including problems related to joints. These considerations are continued in the paper by BASAGLIA *et al.* [3]. Here, local and distortional buckling are also studied. Exemplary calculations are made for L-shaped and portal frames made of open cross-section beams. The possibility of applying GBT-based finite element (FE) calculations to the analysis of frames made of thin-walled members of different cross sections is reported by CAMOTIM *et al.* [4]. The analyses are extended to the non-linear range and the results are compared with those given by the commercial ANSYS code. Possible future developments of the proposed method are also discussed.

The behaviour of frames made of thin-walled members is influenced by the behaviour of their individual elements, i.e., a single beam. For this reason, an optimal shape of the cross section is sought that will provide the highest stiffness and resistance to buckling. Examples of atypical cross sections are presented by MAGNUCKA-BLANDZI and MAGNUCKI [5]. Different types of channel beams are considered. An analytical formula for the critical stress is obtained followed by an optimisation process showing the relation between the geometrical dimensions of the cross section and the critical stress. For selected beams experimental results are shown.

Rectangular frames are parts of vehicle structures and thus subjected to combined loading, mainly bending and torsional moments. The analytical description of the global buckling of such frame made of thin-walled open cross sections is described by MAGNUCKI and MILECKI [6]. The critical values of the forces loading the frame in its plane are determined. The obtained results are compared with those from the finite element method (FEM). Stable and unstable regions of the structure are defined plots.

Large frames in the form of spatial structures are used in construction engineering, e.g., as supporting structures for warehouses. The behaviour of such large frames is analysed by NAGY *et al.* [7]. Three variants of the frame are modelled: a bare frame, a frame with a roof made of trapezoidal sheeting and a frame with a roof made of sandwich panels. Numerical analyses are performed and the differences in the behaviour of these three frames are discussed. The buckling length coefficient for frames was calculated by KRYSTOSIK [8] using three different approaches. The author concluded that the recommendations of the American and European codes, due to assumed simplifications, provide inaccurate results when compared with the FE approach. Thin-walled frames are also

analysed by Zhang *et al.* [9]. A new approach is proposed in which the failure criteria is based on the sum of the structural exponential strain energy density. The buckling of frames and arches made of I cross sections is investigated by Liu *et al.* [10]. An analytical approach based on virtual work is applied to determine the critical loads for different geometries of structures. Different formulations of the joints between particular beams are considered. The effectiveness of the proposed solutions is proved by comparing the results with those obtained by the FEM.

One of the most popular shapes of the beam is the H-section, since it is the most effective one when bending load is considered. The H-section beam under unequal end bending moments is investigated by Giżejowski *et al.* [11]. The influence of the slenderness of the element and moment distribution on the critical state is analysed analytically. Two examples of frames made of H-section and circular section are considered loaded with a static and dynamic loading. The stability of columns and beams with H- and box-sections is analysed by Zhou *et al.* [12]. In the paper, the authors propose a beam-column element with a plastic hinge included making it possible to analyse global and local buckling. Only a single element is needed to predict the load-bearing capacity of columns and frames. Plane frames made of I-sections are investigated analytically by Wen *et al.* [13]. A new comprehensive approach based on the potential energy method is proposed. Different formulas are used to compare their effectiveness in determining the deformation of frames after the loss of stability. An numerical approach to the stability analysis of I-beam is presented by Yang *et al.* [14]. A 1D FE is proposed to solve local and global buckling problems.

Crucial importance for the load-carrying capacity of frames has the connection between particular beam-columns. Such a connection, in the form of K-shaped braced shear panel, is investigated in the paper by Xiang *et al.* [15]. The proposed new connection system is tested in laboratory under seismic load and its ability to dissipate energy is analysed. Experimental tests of frames are also described by Jůza *et al.* [16]. A number of tests are carried out for portal frames made of cold-rolled hollow sections. The influence of material nonlinearity on the deflection of frames is shown. The results are also compared with those from the FE analyses.

If a frame is composed of beams whose thickness is not small or beams that are short, shear stresses play a significant role. The analysis of these stresses is especially important when multilayered beams are considered. An example of research in this area is the work by Magnucki [17]. The author compares the classical zig-zag theory with a new proposal of nonlinear shear deformation theory. It is shown that the stress distribution differs significantly between models based on the two theories. The proposed approach refines the shear effect in multilayered beams. The same theory was applied to analyse the vibrations of

wide-flange H-beam in [18]. The shear coefficient is derived analytically, which refines the formula for natural frequencies. It was shown that this coefficient should be taken into account for short beams, and its application reduces the value of the natural frequency.

In the present paper, the research on the application of the nonlinear shear deformation theory described by MAGNUCKI [17, 18] is continued. Here, the theory is applied to a thin-walled T-frame, shown in Fig. 1a, made of a horizontal H-beam of length $L_1$ and vertical H-beam-column of length $L_2$ rigidly connected together. The joint connecting the two beams of the T-frame is shown in Fig. 1b, where the dimensions of the H-section are presented that is the height of the web – $h$, and the width of the flange – $b$.

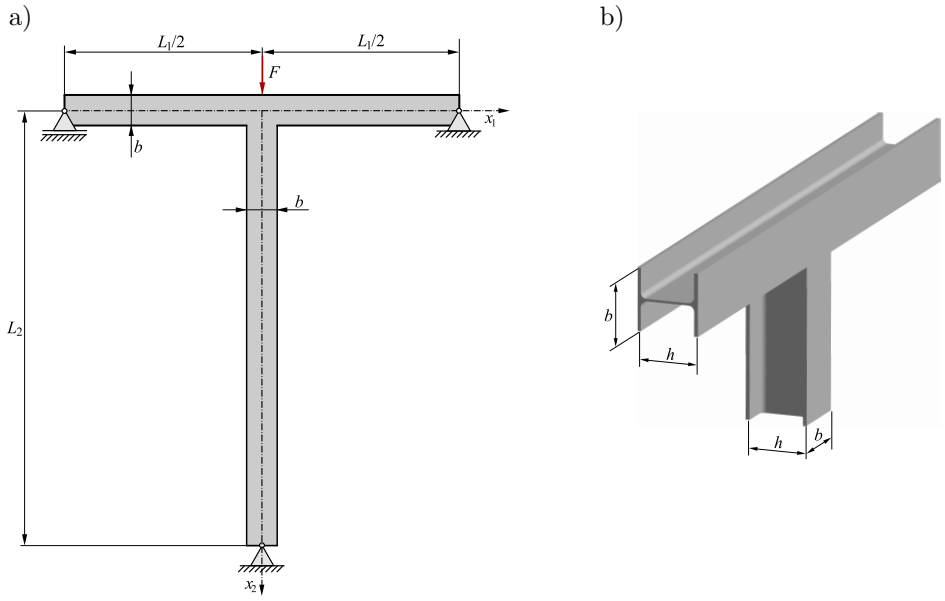


FIG. 1. Scheme of a thin-walled T-frame loaded with a force $F$.

The main goal of the paper is analytical and numerical FEM study of the elastic global buckling problem of the T-frame under the action of force $F$ applied along the centroidal axis of the column.

## 2. Analytical model of the H-beam

The detailed cross section of the H-beam is shown in Fig. 2. The thickness of the flange equals $t_f$ and the thickness of the web is $b_0$. The radius between particular parts of the cross section is equal to $r$.

The analytical description of this cross section is formulated with consideration of the following dimensionless quantities: $\eta = y/b$ – coordinate, $\beta_0 = b_0/b$,

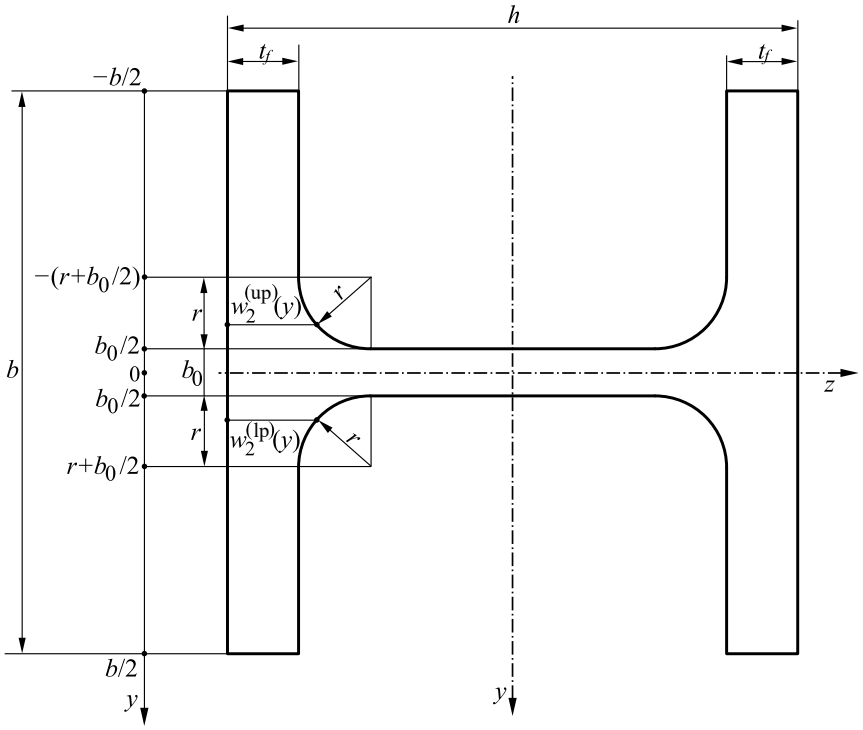


FIG. 2. Scheme of the H-beam cross section.

$\chi_f = t_f/b$, $\rho = r/b$ – dimensionless parameters. Thus, the dimensionless widths $\overline{w}$ of the successive parts:

– the first interval of the upper part $-1/2 \le \eta \le -(\rho + \beta_0/2)$:

$$\overline{w}_1^{(\mathrm{up})}(\eta) = \frac{w_1^{(\mathrm{up})}(\eta)}{b} = 2\chi_f, \tag{2.1}$$

– the second interval of the upper part $-(\rho + \beta_0/2) \le \eta \le -\beta_0/2$:

$$\overline{w}_2^{(\mathrm{up})}(\eta) = \frac{w_2^{(\mathrm{up})}(\eta)}{b} = 2\left\{\chi_f + \rho - \sqrt{-\left(\eta + \frac{1}{2}\beta_0\right)\left(\eta + 2\rho + \frac{1}{2}\beta_0\right)}\right\}, \tag{2.2}$$

– the middle part $-\beta_0/2 \le \eta \le \beta_0/2$:

$$\overline{w}^{(\mathrm{mp})}(\eta) = \frac{w^{(\mathrm{mp})}(\eta)}{b} = \frac{h}{b}, \tag{2.3}$$

– the second interval of the lower part $\beta_0/2 \le \eta \le \rho + \beta_0/2$:

$$\overline{w}_2^{(\mathrm{lp})}(\eta) = \frac{w_2^{(\mathrm{lp})}(\eta)}{b} = 2\left\{\chi_f + \rho - \sqrt{\left(\eta - \frac{1}{2}\beta_0\right)\left(-\eta + 2\rho + \frac{1}{2}\beta_0\right)}\right\}, \tag{2.4}$$

– the first interval of the lower part $\rho + \beta_0/2 \leq \eta \leq 1/2$:

$$\overline{w}_1^{(\mathrm{lp})}(\eta) = \frac{w_1^{(\mathrm{lp})}(\eta)}{b} = 2\chi_f. \tag{2.5}$$

The defined dimensionless widths allow the calculation of geometrical parameters of the cross section, that is, the first moment, necessary for calculated shears stress.

The scheme of the planar cross section deformation of this H-beam after bending-buckling is graphically presented in Fig. 3.

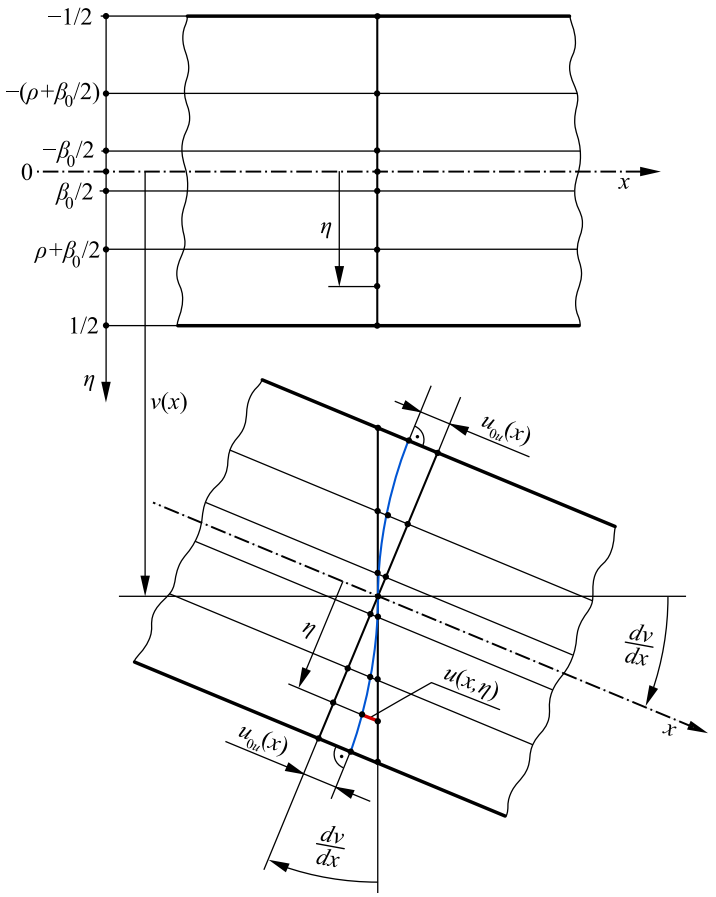


FIG. 3. Scheme of the planar cross section deformation of the H-beam.

The longitudinal displacements $u$, based on the scheme (Fig. 3), and consequently the normal $\varepsilon_x$ and shear $\gamma_{xy}$ strains, as well as normal $\sigma_x$ and shear $\tau_{xy}$ stresses in the successive parts are as follows:

– the first interval of the upper part $-1/2 \le \eta \le -(\rho + \beta_0/2)$:

$$u_1^{(up)}(x,\eta) = -b\left[\eta\frac{dv}{dx} - f_{d1}^{(up)}(\eta)\psi(x)\right], \tag{2.6}$$

$$\varepsilon_{x1}^{(\mathrm{up})}(x,\eta) = -b\left[\eta\frac{d^2v}{dx^2} - f_{d1}^{(\mathrm{up})}(\eta)\frac{d\psi}{dx}\right], \tag{2.7}$$

$$\gamma_{xy1}^{(\mathrm{up})}(x,\eta) = \frac{df_{d1}^{(\mathrm{up})}}{d\eta}\psi(x), \tag{2.8}$$

$$\sigma_{x1}^{(\mathrm{up})}(x,\eta) = E\varepsilon_{x1}^{(\mathrm{up})}(x,\eta), \tag{2.9}$$

$$\tau_{xy1}^{(\mathrm{up})}(x,\eta) = \frac{E}{2(1+\nu)}\gamma_{xy1}^{(\mathrm{up})}(x,\eta), \tag{2.10}$$

– the second interval of the upper part $-(\rho + \beta_0/2) \le \eta \le -\beta_0/2$:

$$u_2^{(\mathrm{up})}(x,\eta) = -b\left[\eta\frac{dv}{dx} - f_{d2}^{(\mathrm{up})}(\eta)\psi(x)\right], \tag{2.11}$$

$$\varepsilon_{x2}^{(\mathrm{up})}(x,\eta) = -b\left[\eta\frac{d^2v}{dx^2} - f_{d2}^{(\mathrm{up})}(\eta)\frac{d\psi}{dx}\right], \tag{2.12}$$

$$\gamma_{xy2}^{(\mathrm{up})}(x,\eta) = \frac{df_{d2}^{(\mathrm{up})}}{d\eta}\psi(x), \tag{2.13}$$

$$\sigma_{x2}^{(\mathrm{up})}(x,\eta) = E\varepsilon_{x2}^{(\mathrm{up})}(x,\eta), \tag{2.14}$$

$$\tau_{xy2}^{(\mathrm{up})}(x,\eta) = \frac{E}{2(1+\nu)}\gamma_{xy2}^{(\mathrm{up})}(x,\eta), \tag{2.15}$$

– the middle part $-\beta_0/2 \le \eta \le \beta_0/2$:

$$u^{(\mathrm{mp})}(x,\eta) = -b\left[\eta\frac{dv}{dx} - f_d^{(\mathrm{mp})}(\eta)\psi(x)\right], \tag{2.16}$$

$$\varepsilon_x^{(\mathrm{mp})}(x,\eta) = -b\left[\eta\frac{d^2v}{dx^2} - f_d^{(\mathrm{mp})}(\eta)\frac{d\psi}{dx}\right], \tag{2.17}$$

$$\gamma_{xy}^{(\mathrm{mp})}(x,\eta) = \frac{df_d^{(\mathrm{mp})}}{d\eta}\psi(x), \tag{2.18}$$

$$\sigma_x^{(\mathrm{mp})}(x,\eta) = E\varepsilon_x^{(\mathrm{mp})}(x,\eta), \tag{2.19}$$

$$\tau_{xy}^{(\mathrm{mp})}(x,\eta) = \frac{E}{2(1+\nu)}\gamma_{xy}^{(\mathrm{mp})}(x,\eta), \tag{2.20}$$

– the second interval of the lower part $\beta_0/2 \le \eta \le \rho + \beta_0/2$:

$$u_2^{(\mathrm{lp})}(x,\eta) = -b\left[\eta\frac{dv}{dx} - f_{d2}^{(\mathrm{lp})}(\eta)\psi(x)\right], \tag{2.21}$$

$$\varepsilon_{x2}^{(\mathrm{lp})}(x,\eta) = -b\left[\eta\frac{d^2v}{dx^2} - f_{d2}^{(\mathrm{lp})}(\eta)\frac{d\psi}{dx}\right], \tag{2.22}$$

$$\gamma_{xy2}^{(\mathrm{lp})}(x,\eta) = \frac{df_{d2}^{(\mathrm{lp})}}{d\eta}\psi(x), \tag{2.23}$$

$$\sigma_{x2}^{(\mathrm{lp})}(x,\eta) = E\varepsilon_{x2}^{(\mathrm{lp})}(x,\eta), \tag{2.24}$$

$$\tau_{xy2}^{(\mathrm{lp})}(x,\eta) = \frac{E}{2(1+\nu)}\gamma_{xy2}^{(\mathrm{lp})}(x,\eta), \tag{2.25}$$

– the first interval of the lower part $\rho + \beta_0/2 \le \eta \le 1/2$:

$$u_1^{(\mathrm{lp})}(x,\eta) = -b\left[\eta\frac{dv}{dx} - f_{d1}^{(\mathrm{lp})}(\eta)\psi(x)\right], \tag{2.26}$$

$$\varepsilon_{x1}^{(\mathrm{lp})}(x,\eta) = -b\left[\eta\frac{d^2v}{dx^2} - f_{d1}^{(\mathrm{lp})}(\eta)\frac{d\psi}{dx}\right], \tag{2.27}$$

$$\gamma_{xy1}^{(\mathrm{lp})}(x,\eta) = \frac{df_{d1}^{(\mathrm{lp})}}{d\eta}\psi(x), \tag{2.28}$$

$$\sigma_{x1}^{(\mathrm{lp})}(x,\eta) = E\varepsilon_{x1}^{(\mathrm{lp})}(x,\eta), \tag{2.29}$$

$$\tau_{xy1}^{(\mathrm{lp})}(x,\eta) = \frac{E}{2(1+\nu)}\gamma_{xy1}^{(\mathrm{lp})}(x,\eta), \tag{2.30}$$

where $f_{d1}^{(\mathrm{up})}(\eta)$, $f_{d2}^{(\mathrm{up})}(\eta)$, $f_{d}^{(\mathrm{mp})}(\eta)$, $f_{d2}^{(\mathrm{lp})}(\eta)$, $f_{d1}^{(\mathrm{lp})}(\eta)$ are unknown dimensionless deformation functions, $v(x)$ is the deflection function, $u_{0u}$ is the longitudinal displacement of the outside surfaces of the beam, $\psi(x) = u_{0u}/h$ is the dimensionless shear effect function, $E$ is Young's modulus, and $\nu$ is Poisson's ratio.

The unknown dimensionless deformation functions are analytically derived in the successive parts and presented further. They are obtained by equating the

shear stresses formulated above with Zhuravsky's classical shear stress formula and by taking into account the first moment of the cross section of the beam. Details of this procedure can be found in [17, 18]. Thus, for particular parts of the cross section there are:

– the first interval of the upper part $-1/2 \le \eta \le -(\rho + \beta_0/2)$:

$$f_{d1}^{(\mathrm{up})}(\eta) = -C_f + \frac{1}{8}\left(1 - \frac{4}{3}\eta^2\right)\eta, \tag{2.31}$$

– the second interval of the upper part $-(\rho + \beta_0/2) \le \eta \le -\beta_0/2$:

$$f_{d2}^{(\mathrm{up})}(\eta) = -C_{up} - C_{p2} + \int\limits_{-(\rho+\beta_0/2)}^{\eta} \frac{\overline{S}_{z2}^{(\mathrm{up})}(\eta)}{\overline{w}_2^{(\mathrm{up})}(\eta)} d\eta, \tag{2.32}$$

– the middle part $-\beta_0/2 \le \eta \le \beta_0/2$:

$$f_{d}^{(\mathrm{mp})}(\eta) = \frac{1}{24}\left(24\frac{b}{h}C_{sz2} + 3\beta_0^2 - 4\eta^2\right)\eta, \tag{2.33}$$

– the second interval of the lower part $\beta_0/2 \le \eta \le \rho + \beta_0/2$:

$$f_{d2}^{(\mathrm{lp})}(\eta) = C_{p2} + \int\limits_{\beta_0/2}^{\eta} \frac{\overline{S}_{z2}^{(lp)}(\eta)}{\overline{w}_2^{(\mathrm{lp})}(\eta)} d\eta, \tag{2.34}$$

– the first interval of the lower part $\rho + \beta_0/2 \le \eta \le 1/2$:

$$f_{d1}^{(\mathrm{lp})}(\eta) = C_f + \frac{1}{8}\left(1 - \frac{4}{3}\eta^2\right)\eta, \tag{2.35}$$

where the dimensionless coefficients are as follows:

$$C_{sz2} = \frac{1}{4}\left[1 - 4\left(\rho + \frac{1}{2}\beta_0^2\right)\right]\chi_f + \int\limits_{-(\rho+\beta_0/2)}^{-\beta_0/2} \overline{w}_2^{\mathrm{up}}(\eta)\eta d\eta,$$

$$C_{p2} = \frac{1}{24}\left(12\frac{b}{h}C_{sz2} + \beta_0^2\right)\beta_0, \qquad C_{p1} = C_{p2} + \int\limits_{\beta_0/2}^{\rho+\beta_0/2} \frac{\overline{S}_{z2}^{(\mathrm{lp})}(\eta)}{\overline{w}_2^{(\mathrm{lp})}(\eta)} d\eta,$$

$$C_{\mathrm{up}} = \int\limits_{-(\rho+\beta_0/2)}^{-\beta_0/2} \frac{\overline{S}_{z2}^{(\mathrm{up})}(\eta)}{\overline{w}_2^{(\mathrm{up})}(\eta)} d\eta, \qquad C_f = C_{p1} - \frac{1}{8}\left[1 - \frac{4}{3}\left(\rho + \frac{1}{2}\beta_0\right)^2\right]\left(\rho + \frac{1}{2}\beta_0\right),$$

and the dimensionless functions are given by

$$\overline{S}_{z2}^{(\mathrm{up})}(\eta) = \frac{1}{4}\left[1 - 4\left(\rho + \frac{1}{2}\beta_0\right)^2\right]\chi_f + \int\limits_{-(\rho+\beta_0/2)}^{\eta} \overline{w}_2^{(\mathrm{up})}(\eta)\eta d\eta,$$

$$\overline{S}_{z2}^{(\mathrm{lp})}(\eta) = C_{sz2} + \frac{1}{4}\left(\beta_0^2 - 4\eta^2\right)(\chi_f + \rho) + \int\limits_{-(\rho+\beta_0/2)}^{\eta} \overline{w}_2^{(\mathrm{up})}(\eta)\eta d\eta.$$

These dimensionless deformation functions satisfy the continuity conditions between the successive parts of the cross section.

To solve the stability problem, the principle of stationary total potential energy will be used in the form $\delta(U_{\varepsilon\gamma} - W) = 0$ (for details see [17]). The elastic strain energy $U_{\varepsilon\gamma}$ of the horizontal and vertical beam is defined as well as the work $W$ of external load. After substituting them into the principle of stationary total potential energy and performing simple transformation, the system of two differential equations of equilibrium for this H-beam is obtained in the following form:

$$\overline{J}_z \frac{d^2v}{dx^2} - C_{v\psi}\frac{d\psi}{dx} = -\frac{M_b(x)}{Eb^3h}, \tag{2.36}$$

$$C_{v\psi}\frac{d^3v}{dx^3} - C_{\psi\psi}\frac{d^2\psi}{dx^2} + C_{\psi}\frac{\psi(x)}{bh} = 0, \tag{2.37}$$

where the dimensionless coefficients are as follows:

$$\overline{J}_z = \frac{1}{12}\beta_0^3 + \frac{1}{6}\left[1 - 8\left(\rho + \frac{1}{2}\beta_0\right)^3\right]\frac{b}{h}\chi_f + 2\frac{b}{h}\int\limits_{\beta_0/2}^{\rho+\beta_0/2} \eta^2\overline{w}_2^{(\mathrm{lp})}(\eta)d\eta,$$

$$C_{v\psi} = \int\limits_{-\beta_0/2}^{\beta_0/2} \eta f_d^{(\mathrm{mp})}(\eta)d\eta + 2\frac{b}{h}\left\{\int\limits_{\beta_0/2}^{\rho+\beta_0/2} \eta f_{d2}^{(\mathrm{lp})}(\eta)\overline{w}_2^{(\mathrm{lp})}(\eta)d\eta + 2\chi_f\int\limits_{\rho+\beta_0/2}^{1/2} \eta f_{d1}^{(\mathrm{lp})}(\eta)d\eta\right\},$$

$$C_{\psi\psi} = \int\limits_{-\beta_0/2}^{\beta_0/2} \left[f_d^{(\mathrm{mp})}(\eta)\right]^2 d\eta + 2\frac{b}{h}\left\{\int\limits_{\beta_0/2}^{\rho+\beta_0/2} \left[f_{d2}^{(\mathrm{lp})}(\eta)\right]^2 \overline{w}_2^{(\mathrm{lp})}(\eta)d\eta + 2\chi_f\int\limits_{\rho+\beta_0/2}^{1/2} \left[f_{d1}^{(\mathrm{lp})}(\eta)\right]^2 d\eta\right\},$$

$$C_\psi = \frac{1}{2(1+\nu)} \left\{ \int\limits_{-\beta_0/2}^{\beta_0/2} \left[ \frac{b}{h} C_{sz2} + \frac{1}{8} \left( \beta_0^2 - 4\eta^2 \right) \right]^2 d\eta \right.$$
$$\left. + 2\frac{b}{h} \int\limits_{\beta_0/2}^{\rho+\beta_0/2} \frac{\left[ \overline{S}_{z2}^{(\mathrm{lp})}(\eta) \right]^2}{\overline{w}_2^{(\mathrm{lp})}(\eta)} d\eta + \frac{\chi_f}{16} \frac{b}{h} \int\limits_{\rho+\beta_0/2}^{1/2} \left( 1 - 4\eta^2 \right)^2 d\eta \right\}.$$

These two differential equations of equilibrium, (2.36) and (2.37), are fundamental in the analysis of the T-frame buckling problem.

## 3. Analytical model of the thin-walled T-frame taking into account the shear effect

### 3.1. Pre-buckling state

The T-frame is a statically indeterminate structure. The disconnected beams with the interaction force $F_c$ are shown in Fig. 4. The detailed scheme of the

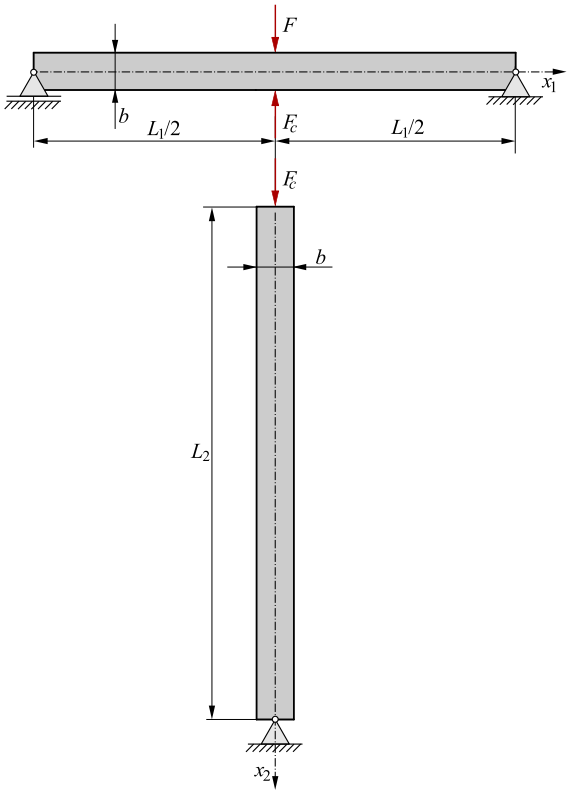


Fig. 4. Scheme of the interaction force $F_c$ of two beams.

horizontal beam subjected to loading is shown in Fig. 5. The bending moment based on this scheme is as follows:

$$M_b(\xi_1) = \frac{1}{2}\xi_1 \left(F - F_c\right) b\lambda_1, \tag{3.1}$$

where $\xi_1 = x_1/L_1$ is the dimensionless coordinate ($0 \leq \xi_1 \leq 1/2$) and $\lambda_1 = L_1/b$ is the relative length of the horizontal beam.

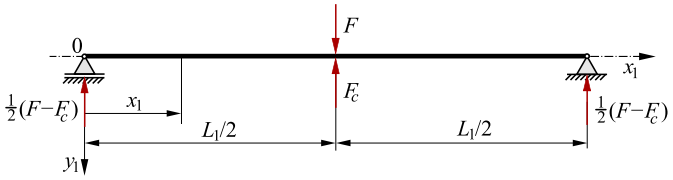


FIG. 5. Scheme of the horizontal beam with the load.

Thus, the equations of equilibrium, (2.36) and (2.37), expressed in terms of the dimensionless coordinate $\xi_1$, with consideration of Eq. (3.1), are in the following form:

$$\overline{J}_z \frac{d^2 v}{d\xi_1^2} - C_{v\psi} L_1 \frac{d\psi_{11}}{d\xi_1} = -\frac{1}{2}\xi_1 \lambda_1^3 \frac{F - F_c}{Eh}, \tag{3.2}$$

$$C_{v\psi} \frac{d^3 v}{d\xi_1^3} - C_{\psi\psi} L_1 \frac{d^2\psi_{11}}{d\xi_1^2} + C_{\psi} \lambda_1^2 L_1 \frac{b}{h} \psi_{11}(\xi_1) = 0, \tag{3.3}$$

Equation (3.2) and Eq. (3.3), after simple transformation, are reduced to a single equation in the form:

$$\frac{d^2\psi_{11}}{d\xi_1^2} - \alpha^2 \lambda_1^2 \frac{b}{h} \psi_{11}(\xi_1) = -\frac{1}{2}\lambda_1^2 \frac{C_{v\psi}}{\overline{J}_z C_{\psi\psi} - C_{v\psi}^2} \frac{F - F_c}{Ebh}, \tag{3.4}$$

where $\alpha = \sqrt{\dfrac{\overline{J}_z C_{\psi}}{\overline{J}_z C_{\psi\psi} - C_{v\psi}^2}}$ is the dimensionless coefficient. The solution of Eq. (3.4) is given by the following function:

$$\psi_{11}(\xi_1) = \frac{1}{2}\left\{1 - \frac{\cosh\left(\alpha\lambda_1\sqrt{b/h}\xi_1\right)}{\cosh\left(0.5\alpha\lambda_1\sqrt{b/h}\right)}\right\} \frac{C_{v\psi}}{\overline{J}_z C_{\psi}} \frac{F - F_c}{Eb^2}. \tag{3.5}$$

This function satisfies the conditions: $d\psi_1/d\xi_1\big|_0 = 0$ and $\psi_1(1/2) = 0$. Substituting function (3.5) into Eq. (3.2), after integration and simple transformation, one obtains the beam deflection line:

$$v(\xi_1) = \left[\left(\xi_1 - \frac{4}{3}\xi_1^3\right)\frac{b}{h} + \frac{8}{\lambda_1^2} f_{v\psi}(\xi_1) \frac{C_{v\psi}^2}{\overline{J}_z C_{\psi}}\right] \frac{\lambda_1^3}{16\overline{J}_z} \frac{F - F_c}{Eb}, \tag{3.6}$$

where

$$f_{v\psi}(\xi_1) = \xi_1 - \frac{\sinh\left(\alpha\lambda_1\sqrt{b/h}\xi_1\right)}{\alpha\lambda_1\sqrt{b/h}\cosh\left(0.5\alpha\lambda_1\sqrt{b/h}\right)}.$$

Function (3.6) satisfies the conditions: $dv/d\xi_1\big|_{1/2} = 0$ and $v(0) = 0$. Thus, the maximum deflection of the horizontal beam is as follows:

$$v_1 = (1 + C_{se1})\frac{\lambda_1^3}{48\overline{J}_z}\frac{F - F_c}{Eh}, \tag{3.7}$$

where the dimensionless shear coefficient:

$$C_{se1} = \frac{12}{\lambda_1^2}\frac{h}{b}\left[1 - \frac{2}{\alpha\lambda_1}\sqrt{\frac{h}{b}}\tanh\left(\frac{1}{2}\alpha\lambda_1\sqrt{\frac{b}{h}}\right)\right]\frac{C_{v\psi}^2}{\overline{J}_z C_\psi}. \tag{3.8}$$

The shortening of the vertical H-beam-column under the action of force $F_c$ (Fig. 4) is as follows:

$$\Delta L_2 = \frac{F_c\lambda_2}{E\overline{A}h}, \tag{3.9}$$

where

$$\overline{A} = \beta_0 + 2\left\{\left[1 - 2\left(\rho + \frac{1}{2}\beta_0\right)\right]\chi_f + \int_{\beta_0/2}^{\rho+\beta_0/2}\overline{w}_2^{(\mathrm{lp})}(\eta)d\eta\right\}\frac{b}{h}$$

is the dimensionless cross section area, and $\lambda_2 = L_2/b$ is the relative length of the beam-column.

Based on the condition $v_1 = \Delta L_2$, which states that the deflection of the horizontal beam is consistent with the shortening of the beam-column, one obtains the force:

$$F_c = \frac{(1 + C_{se1})\overline{A}\lambda_1^3}{48\overline{J}_z\lambda_2 + (1 + C_{se1})\overline{A}\lambda_1^3}F. \tag{3.10}$$

### 3.2. Buckling state

The form of the horizontal H-beam bending line of the T-frame after its buckling is shown in Fig. 6. The bending moment, based on this scheme, in the dimensionless coordinate $\xi_1 = x_1/L_1$ for the first interval $(0 \le \xi_1 \le 1/2)$, is as follows:

$$M_b(\xi_1) = -\xi_1 M_0, \tag{3.11}$$

where $M_0$ is the moment at the joint connecting the two beams.

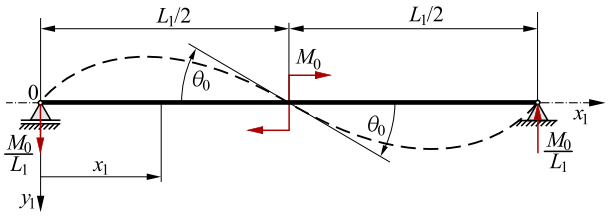


FIG. 6. Scheme of the deflection line of the horizontal H-beam.

Therefore, the equation of equilibrium (2.36) in the dimensionless coordinate $\xi_1$, with consideration of Eq. (3.11), is in the following form:

$$\overline{J}_z \frac{d^2v}{d\xi_1^2} - C_{v\psi} L_1 \frac{d\psi_{12}}{d\xi_1} = \xi_1 \lambda_1^2 \frac{M_0}{Ebh}. \tag{3.12}$$

However, Eq. (2.37) is of the form of Eq. (3.3), with the dimensionless function $\psi_{12}(\xi_1)$. Solving Eq. (3.12) and Eq. (3.3), after simple transformation, one obtains the dimensionless function:

$$\psi_{12}(\xi_1) = -\left\{1 - \frac{\cosh\left(\alpha\lambda_1\sqrt{b/h}\xi_1\right)}{\cosh\left(0.5\alpha\lambda_1\sqrt{b/h}\right)}\right\} \frac{C_{v\psi}}{\overline{J}_z C_\psi} \frac{1}{\lambda_1} \frac{M_0}{Eb^3}, \tag{3.13}$$

and the rotation angle of the center of the deflection line:

$$\theta_0 = (1 + C_{se1}) \frac{\lambda_1}{12\overline{J}_z} \frac{b}{h} \frac{M_0}{Eb^3}, \tag{3.14}$$

where $C_{se1}$ is the dimensionless shear coefficient consistent with Eq. (3.8).

The buckling line form of the vertical H-beam-column is shown in Fig. 7. The bending moment, based on this scheme, in the dimensionless coordinate, is as follows:

$$M_b(\xi_2) = -(1 - \xi_2)M_0 + F_c v(\xi_2), \tag{3.15}$$

where $\xi_2 = x_2/L_2$ is the dimensionless coordinate $(0 \leq \xi_2 \leq 1)$, $\lambda_2 = L_2/b$ is the relative length of the vertical beam-column.

Consequently, the equilibrium Eq. (2.36) and Eq. (2.37), in the dimensionless coordinate $\xi_2$, with consideration of the bending moment (3.15), are in the following form:

$$\overline{J}_z \frac{d^2v}{d\xi_2^2} - C_{v\psi} L_2 \frac{d\psi_2}{d\xi_2} = \left[(1 - \xi_2)M_0 - F_c v(\xi_2)\right] \lambda_2^2 \frac{1}{Ebh}, \tag{3.16}$$

$$C_{v\psi} \frac{d^3v}{d\xi_2^3} - C_{\psi\psi} L_{12} \frac{d^2\psi_2}{d\xi_2^2} + C_\psi \lambda_2^2 L_2 \frac{b}{h} \psi_2(\xi_2) = 0. \tag{3.17}$$

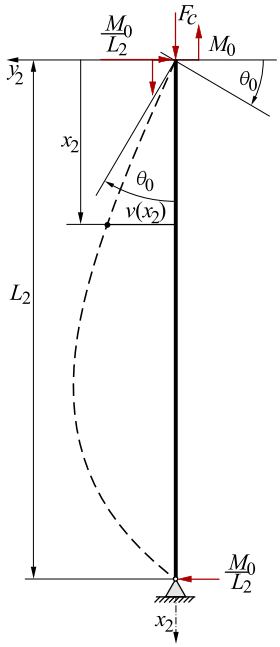


FIG. 7. Scheme buckling line form of the vertical H-beam-column.

These two differential equations, after simple transformations, are reduced to a fourth-order differential equation in the following form:

$$\frac{d^4v}{d\xi_2^4} - k_1\frac{d^2v}{d\xi_2^2} - k_2 v(\xi_2) = -(1-\xi_2)\alpha^2\frac{\lambda_2^4}{\overline{J}_z}\left(\frac{b}{h}\right)^2\frac{M_0}{Eb^2}, \tag{3.18}$$

where $k_1 = \alpha^2\lambda_2^2\dfrac{b}{h}\left(1 - \dfrac{C_{v\psi}}{\overline{J}_z C_\psi}\overline{F}_c\right)$ and $k_2 = \alpha^2\dfrac{\lambda_2^4}{\overline{J}_z}\left(\dfrac{b}{h}\right)^2\overline{F}_c$ are the dimensionless coefficients, and $\overline{F}_c = F_c/Eb^2$ is the dimensionless force.

Solving Eq. (3.18), taking into account the boundary conditions $v(0) = v(1) = 0$, one obtains the buckling line of the vertical beam-column in the form:

$$v(\xi_2) = \left\{1 - \xi_2 - \frac{\sin\left[(1-\xi_2)p\right]}{\sin(p)}\right\}\frac{1}{\overline{F}_c}\frac{M_0}{Eb^2}, \tag{3.19}$$

where $p = \frac{1}{\sqrt{2}}\sqrt{-k_1 + \sqrt{k_1^2 + 4k_2}}$ is the dimensionless coefficient. Consequently, the rotation angle at the beginning of this line ($\xi_2 = 0$) is as follows:

$$\theta_0 = \left.\frac{dv}{L_2 d\xi_2}\right|_0 = \left[\frac{p}{\tan(p)} - 1\right]\frac{1}{\overline{F}_c}\frac{1}{\lambda_2}\frac{M_0}{Eb^3}. \tag{3.20}$$

By equating the rotation angles (3.14) and (3.20), one obtains the algebraic equation:

$$(1+C_{se1})\frac{\lambda_1}{12}\frac{\lambda_2}{\overline{J}_z}\frac{b}{h}\overline{F}_c+1-\frac{p}{\tan(p)}=0. \tag{3.21}$$

Based on Eq. (3.21), the dimensionless critical force $\overline{F}_{c,\mathrm{CR}}$ for the vertical beam-column alone is determined, and consequently, taking into account Eq. (3.10), one obtains the dimensionless critical force for the whole frame:

$$\overline{F}_{\mathrm{CR}}=\left[1+\frac{48\overline{J}_z\lambda_2}{(1+C_{se1})\overline{A}\lambda_1^3}\right]\overline{F}_{c,\mathrm{CR}}. \tag{3.22}$$

## 4. Analytical model of the thin-walled T-frame neglecting shear effect

This presented frame model is a simplification of the model presented in Sec. 3 and is developed on the basis of the Bernoulli–Euler beam theory.

### 4.1. Pre-buckling state

Equation (3.2), describing the horizontal beam bending in the first interval $(0\le\xi_1\le 1/2)$ (Fig. 5), without the dimensionless shear effect function $\psi_{11}(\xi_1)$, is in the following form:

$$\overline{J}_z\frac{d^2v}{d\xi_1^2}=-\frac{1}{2}\xi_1\lambda_1^3\frac{F^{(o)}-F_c^{(o)}}{Eh}, \tag{4.1}$$

where the superscript $(o)$ in the forces refers to the variant without the shear effect. After integrating this equation twice and taking into account the following conditions: $v(0)=0$ and $dv/d\xi_1|_{1/2}=0$, one obtains the deflection line in the form:

$$v\left(\xi_1\right)=\left(3-4\xi_1^2\right)\xi_1\frac{\lambda_1^3}{48\overline{J}_z}\frac{F^{(o)}-F_c^{(o)}}{Eh}. \tag{4.2}$$

Thus, the maximum deflection of this beam is as follows:

$$v_1=v\left(\frac{1}{2}\right)=\frac{\lambda_1^3}{48\overline{J}_z}\frac{F^{(o)}-F_c^{(o)}}{Eh}. \tag{4.3}$$

It is easy to see that this expression is the same as Eq. (3.7) for $C_{se1}=0$, when the shear effect is omitted.

The shortening of the vertical H-beam-column under the action of the force (Fig. 5) is in the form of Eq. (3.9). Based on the condition $v_1 = \Delta L_2$, one obtains the relationship between the forces $F_c^{(o)}$ and $F^{(o)}$ in the form:

$$F_c^{(o)} = \frac{\overline{A}\lambda_1^3}{48\overline{J}_z\lambda_2 + \overline{A}\lambda_1^3} F^{(o)}, \tag{4.4}$$

or

$$F^{(o)} = \left(1 + \frac{48\overline{J}_z\lambda_2}{\overline{A}\lambda_1^3}\right) F_c^{(o)}. \tag{4.5}$$

It is easy to see that Eq. (4.4) is the same as Eq. (3.10) for $C_{se1} = 0$, when the shear effect is omitted.

### 4.2. Buckling state

Taking into account Fig. 6, and Eq. (3.12), without the dimensionless shear effect function $\psi_{12}(\xi_1)$, the equilibrium equation is in the following form:

$$\overline{J}_z \frac{d^2v}{d\xi_1^2} = \xi_1\lambda_1^2 \frac{M_0^{(o)}}{Ebh}. \tag{4.6}$$

Integrating Eq. (4.6) twice and taking into account the conditions: $v(0) = 0$ and $v(1/2) = 0$, one obtains the horizontal beam deflection line in the form:

$$v(\xi_1) = -\left(1 - 4\xi_1^2\right)\xi_1 \frac{\lambda_1^2}{24\overline{J}_z} \frac{M_0^{(o)}}{Eb^2h}, \tag{4.7}$$

and consequently, the slope of this beam deflection line is as follows:

$$\frac{dv}{L_1 d\xi_1} = \left(12\xi_1^2 - 1\right) \frac{\lambda_1}{24\overline{J}_z} \frac{M_0^{(o)}}{Eb^2h}. \tag{4.8}$$

Thus, the rotation angle at the center of the deflection line is as follows:

$$\theta_0 = \left.\frac{dv}{L_1 d\xi_1}\right|_{1/2} = \frac{\lambda_1}{12\overline{J}_z} \frac{1}{h} \overline{M}_0^{(o)}, \tag{4.9}$$

where $\overline{M}_0^{(o)} = M_0^{(o)}/Eb^2$ is the dimensionless moment. It is easy to see that this expression is the same as Eq. (3.14) for $C_{se1} = 0$, when the shear effect is omitted.

Taking into account Fig. 7, and Eq. (3.16), without the dimensionless shear effect function $\psi_2(\xi_2)$, after simple transformation, the governing equation is in the following form:

$$\frac{d^2v}{d\xi_2^2} + \frac{\lambda_2^2}{\overline{J}_z}\frac{b}{h}\overline{F}_c^{(o)} v(\xi_2) = (1-\xi_2)\frac{\lambda_2^2}{\overline{J}_z}\frac{b}{h}\overline{M}_0^{(o)}, \tag{4.10}$$

where $\overline{F}_c^{(o)} = F_c^{(o)}/Eb^2$ is the dimensionless force. Solving this second-order differential equation, taking into account two boundary conditions $v(0) = v(1) = 0$, after simple transformation, one obtains the buckling line of the vertical beam-column in the form:

$$v(\xi_2) = \left\{1 - \xi_2 - \frac{\sin\left[(1-\xi_2)\,p^{(o)}\right]}{\sin\left(p^{(o)}\right)}\right\}\frac{\overline{M}_0^{(o)}}{\overline{F}_c^{(o)}}, \tag{4.11}$$

where $p^{(o)} = \lambda_2\sqrt{\frac{b}{h}\frac{\overline{F}_c^{(o)}}{\overline{J}_z}}$ is the dimensionless coefficient.

The slope of this buckling line is as follows:

$$\frac{dv}{L_2 d\xi_2} = \left\{-1 + f_{\mathrm{CR}}\frac{\cos\left[(1-\xi_2)\,p^{(o)}\right]}{\sin\left(p^{(o)}\right)}\right\}\frac{\overline{M}_0^{(o)}}{L_2\overline{F}_c^{(o)}}. \tag{4.12}$$

Thus, the rotation angle at the beginning of this buckling line is as follows:

$$\theta_0 = \left.\frac{dv}{L_2 d\xi_1}\right|_0 = \left[\frac{p^{(o)}}{\tan\left(p^{(o)}\right)} - 1\right]\frac{\overline{M}_0^{(o)}}{L_2\overline{F}_c^{(o)}}. \tag{4.13}$$

By equating the rotations angles (4.9) and (4.13), one obtains the algebraic equation:

$$\frac{\lambda_1\lambda_2}{12\overline{J}_z}\frac{b}{h}\overline{F}_{c,\mathrm{CR}}^{(o)} + 1 - \frac{p^{(o)}}{\tan\left(p^{(o)}\right)} = 0. \tag{4.14}$$

Based on Eq. (4.14), the dimensionless critical force $F_{c,\mathrm{CR}}^{(o)}$ for the vertical beam-column is determined, and in accordance with Eq. (4.5), one obtains the dimensionless critical force for the T-frame without shear effect:

$$\overline{F}_{\mathrm{CR}}^{(o)} = \left(1 + \frac{48\overline{J}_z\lambda_2}{\overline{A}\lambda_1^3}\right)\overline{F}_{c,\mathrm{CR}}^{(o)}. \tag{4.15}$$

It is easy to see that this expression is the same as Eq. (3.22) for $C_{se1} = 0$, when the shear effect is omitted.

## 5. Analytical studies of selected T-frames

Example analytical studies are carried out for a thin-walled T-frame made of a horizontal beam with relative lengths $\lambda_1 = 10, 15, 20, 30, 40$, and a vertical beam-column with relative length $\lambda_2 = 40$. Sizes of three standard H-beams are shown in Table 1.

Table 1. Dimensions of the three selected standard H-beams.

| Sizes | $h$ [mm] | $b$ [mm] | $b_0$ [mm] | $t_f$ [mm] | $r$ [mm] |
|---|---|---|---|---|---|
| H-300 | 300 | 300 | 11.0 | 19.0 | 27.0 |
| H-400 | 400 | 300 | 13.5 | 24.0 | 27.0 |
| H-500 | 500 | 300 | 14.5 | 28.0 | 27.0 |

The values of the dimensionless critical forces calculated on the basis of Eq. (3.21) and Eq. (3.22) for the case of shear effect taken into account and Eq. (4.14) and Eq. (4.15), neglecting this effect are presented in Table 2, Table 3, and Table 4.

Table 2. Critical forces of T-frame made of standard H-300 beams.

| $\lambda_1$ | 10 | 15 | 20 | 30 | 40 |
|---|---|---|---|---|---|
| $10^4\overline{F}_{c,\mathrm{CR}}$ | 1.24240 | 1.22063 | 1.19980 | 1.16123 | 1.12664 |
| $10^4\overline{F}^{(o)}_{c,\mathrm{CR}}$ | 1.28132 | 1.25771 | 1.23422 | 1.19230 | 1.15505 |
| $10^4\overline{F}_{\mathrm{CR}}$ | 1.39063 | 1.26442 | 1.21805 | 1.16648 | 1.12880 |
| $10^4\overline{F}^{(o)}_{\mathrm{CR}}$ | 1.43833 | 1.30273 | 1.25312 | 1.19771 | 1.15726 |

Table 3. Critical forces of T-frame made of standard H-400 beams.

| $\lambda_1$ | 10 | 15 | 20 | 30 | 40 |
|---|---|---|---|---|---|
| $10^4\overline{F}_{c,\mathrm{CR}}$ | 1.55404 | 1.52748 | 1.50195 | 1.45453 | 1.41189 |
| $10^4\overline{F}^{(o)}_{c,\mathrm{CR}}$ | 1.61894 | 1.58832 | 1.55942 | 1.50646 | 1.45940 |
| $10^4\overline{F}_{\mathrm{CR}}$ | 1.72912 | 1.57947 | 1.52337 | 1.46080 | 1.41446 |
| $10^4\overline{F}^{(o)}_{\mathrm{CR}}$ | 1.80787 | 1.64324 | 1.58217 | 1.51297 | 1.46206 |

Table 4. Critical forces of T-frame made of standard H-500 beams.

| $\lambda_1$ | 10 | 15 | 20 | 30 | 40 |
|---|---|---|---|---|---|
| $10^4\overline{F}_{c,\mathrm{CR}}$ | 1.79638 | 1.76636 | 1.73741 | 1.68347 | 1.63484 |
| $10^4\overline{F}^{(o)}_{c,\mathrm{CR}}$ | 1.88901 | 1.85329 | 1.81957 | 1.75777 | 1.70286 |
| $10^4\overline{F}_{\mathrm{CR}}$ | 1.99066 | 1.82430 | 1.76165 | 1.69048 | 1.63777 |
| $10^4\overline{F}^{(o)}_{\mathrm{CR}}$ | 2.10220 | 1.91526 | 1.84523 | 1.76512 | 1.70586 |

By comparing the values of critical forces determined analytically with and without taking into account the shear effect, it is easy to see that the shear effect reduces the values of the critical forces. Differences between these values of critical forces are specified in Table 5.

TABLE 5. Differences between the values of critical forces with and without the shear effect.

| $\lambda_1$ | 10 | 15 | 20 | 30 | 40 |
|---|---|---|---|---|---|
| $\Delta\overline{F}_{\mathrm{CR}}^{(\mathrm{H}-300)}\%$ | 3.4 | 3.0 | 2.9 | 2.7 | 2.5 |
| $\Delta\overline{F}_{\mathrm{CR}}^{(\mathrm{H}-400)}\%$ | 4.6 | 4.0 | 3.9 | 3.6 | 3.4 |
| $\Delta\overline{F}_{\mathrm{CR}}^{(\mathrm{H}-500)}\%$ | 5.6 | 5.0 | 4.7 | 4.4 | 4.2 |

Moreover, these results of the exemplary calculations are graphically presented in the next section and compared with the results of FE analyses.

## 6. NUMERICAL (FEM) STUDIES OF SELECTED T-FRAMES

As a comparative study a FE analysis is performed. A 3D model of the whole frame is prepared. A linear buckling analysis is carried out using the Ansys[1)] software. The material model is assumed to be linear elastic with the following parameters: Young's modulus $E = 200\,000$ MPa and Poisson's ratio $\nu = 0.3$. The boundary conditions applied to the model are shown in Fig. 8a. All three

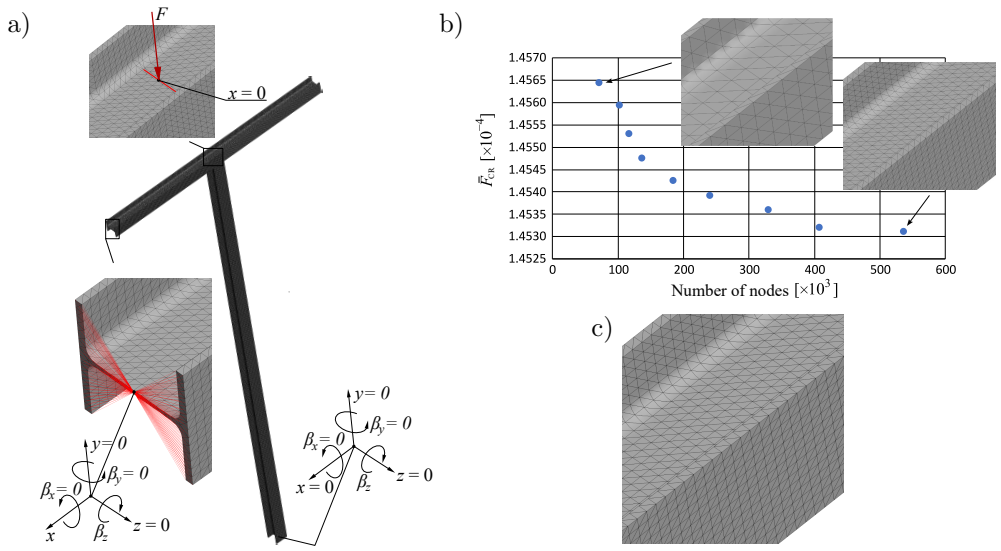


FIG. 8. FE model of the T-frame: a) boundary conditions, b) mesh convergence study, c) mesh pattern.

[1)] Ansys, Inc., Academic Research Mechanical Release 2023 R2.

ends of the frame are pin-supported. A remote displacement option was used to achieve this condition, which was applied to the whole cross section and realised at its centroid. At the bottom of the vertical part of the frame, displacements along three axes are blocked. Rotation about the $z$-axis is allowed. Both ends of the horizontal part can move horizontally and rotate about the $z$-axis. To avoid rigid-body motion, the horizontal displacement is taken away at one node at the mid-length of the horizontal beam. The force $F$ is applied to the upper part of this beam, at the edge corresponding to the center line of the web of the vertical part of the frame (see Fig. 8a).

To discretise the model of the frame, solid elements are used marked as *SOLID186* which were tetrahedral, second-order FEs with 10 nodes and 3 degrees-of-freedom in each node – displacements in three directions. This choice provides the most effective model among those investigated, in which both tetrahedral and hexahedral elements were taken into account. The negative influence of using a single element over the thickness of the beam wall was also verified. The number of elements was established based on the mesh convergence analysis presented in Fig. 8b. It was decided to set the element size to 22, which gave about 400 000 nodes for the H-300 frame with the parameter $\lambda_1 = 10$. It should be noted that even for the two extreme cases considered, shown in Fig. 8b, the difference in value of the buckling load is only about 0.2 %. This comes from the fact that the buckling mode has a global character and the analysis is a linear one. The exemplary mesh used in all analyses is shown in Fig. 8c.

Typical buckling shapes corresponding to the H-300 frame are shown in Fig. 9 for selected lengths of the horizontal beam. The values of the buckling load for all considered frames are presented in Fig. 10, together with the results given by the analytical solution described in Sec. 5. They are given on the vertical axis whereas the horizontal axis corresponds to the length parameter $\lambda_1$ – the higher

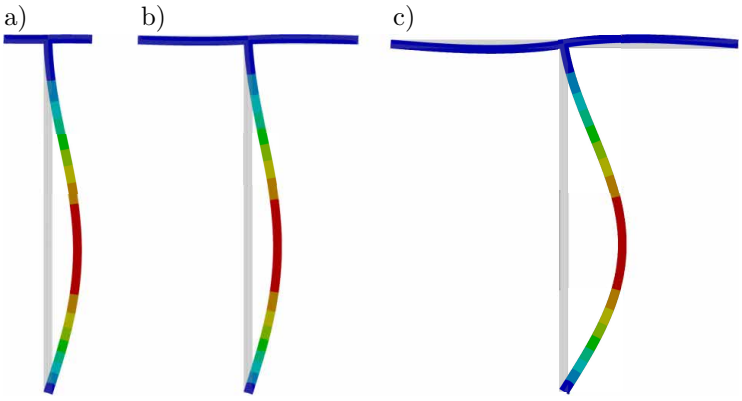


FIG. 9. First buckling mode of the H-300 T-frame for different $\lambda_1$: a) $\lambda_1 = 10$, b) $\lambda_1 = 25$, c) $\lambda_1 = 40$ (scaled $10^3$).

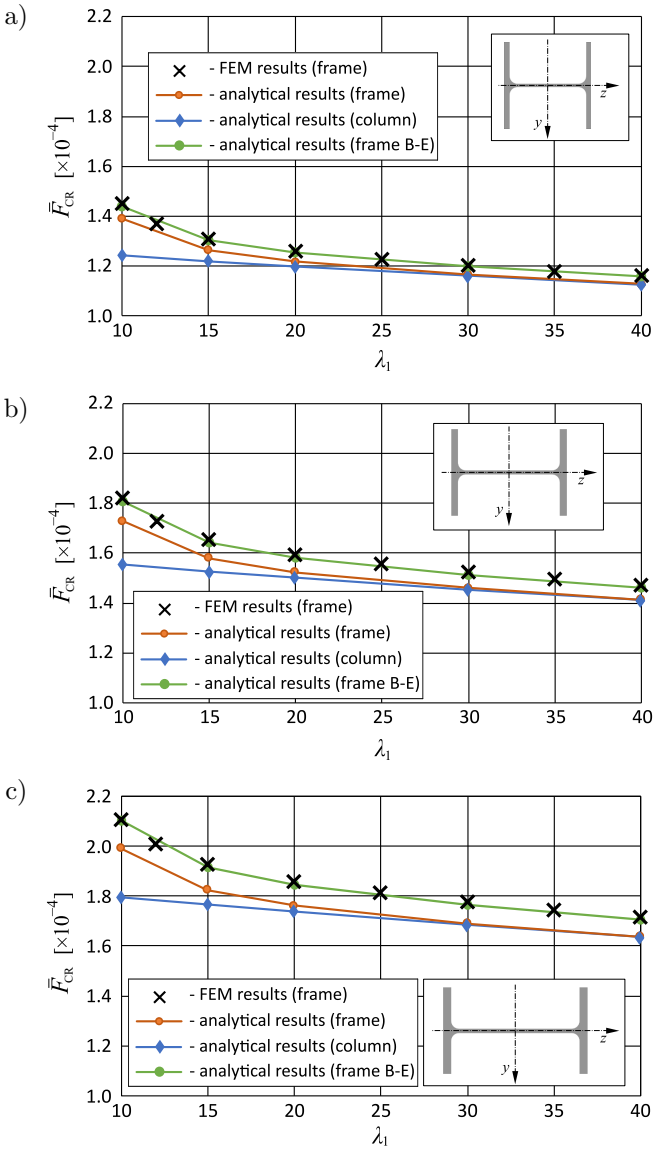


FIG. 10. Comparison of dimensionless buckling loads obtained with analytical and numerical approach: a) H-300, b) H-400, c) H-500.

its value, the longer the horizontal part of the frame. Regarding the analytical solution, two curves are shown. One of them corresponds to the buckling load for the whole frame – red line with circles, and the second one corresponds to the buckling of the vertical beam only – blue line with diamonds. In the FE analysis, only the whole frame was analysed and the results are marked with black crosses.

## 7. Discussion of the results

The presented results were obtained with the use of both the analytical model and numerical approach. In both cases linear behaviour of the material was assumed. In analytical model the shear stresses were taken into account.

For all considered examples, the shape of the frame after the loss of stability was the same and consistent with those shown in Fig. 9, in which the presented deformation is magnified $10^3$ times for better visualisation. The vertical part buckles such as the column hinged supported at the bottom and either hinged or rigidly supported at the top. The latter depended on the length of the horizontal beam. If the beam is short it behaves similarly to the fixed support, and the rotation at this point is small. The longer the beam, the smaller its influence on the behaviour of the column, which will deform as hinged/supported column at both ends if the beam is long enough. This relationship is also visible in the values of the buckling loads obtained from the analytical solution. The longer the horizontal beam, the closer the value of the buckling load of the frame (red line in Fig. 10) is to the value corresponding to the case when only the column is considered (blue line). In the presented examples for $\lambda_1 = 40$, the buckling load for the frame is only 0.2 % higher than that of the column. This means that the influence of the horizontal beam on the stability of the whole structure is negligible.

The distribution of the results given by the FE analyses (black crosses in Fig. 10) is similar to those from the analytical solution. They are slightly above the red curve. The smallest difference was noted for the H-300 frame with $\lambda_1 = 40$ and was equal to 3 % and the biggest difference, 6 %, was observed for the H-500 frame with $\lambda_1 = 10$. However, the FE results are very close to the analytical solution in which shear effect is omitted (green line – B-E) – the discrepancy does not exceed 1 %. Since the influence of the FE type on the results was eliminated and a number of boundary conditions were verified, the agreement between the FE results and the B-E theory may be the result of the linear nature of the buckling analysis, which is not able to capture the shear effect phenomenon.

## 8. Conclusions

In the present work, the problem of stability of the T-frame was solved analytically and numerically. The novelty of the analytical approach proposed in the paper lies in the fact that the influence of shear stress on the deformation of the frame is taken into account in the model definition. This makes the analytical calculations more realistic, especially when short beams are considered, and at the same time makes the structure safer. The defined shear coefficient

allows the contribution of shear stress to the critical load to be determined. The presented formulae give more conservative results even when compared with the numerical calculations since the inclusion of the shear effect reduces the stiffness of the structure and thus lowers the value of the buckling load. The obtained buckling loads are consistent for both approaches and the biggest difference between the analytical and numerical solution is equal to 6 %. Additional FE analyses have to be performed regarding the compatibility of both methods with emphasis on FE modelling details such as the type and number of elements or the method of applying the load and supports.

The presented approach has a general form and can be applied to different shapes of cross section. Further extensive investigation, including experimental tests, may validate its correctness and explain the influence of shear stress on the behaviour of engineering structures.

## Fundings

The paper is developed based on the scientific activity of the Łukasiewicz Research Network – Poznan Institute of Technology and the statutory activity of the Poznan University of Technology (Grant of the Ministry of Science and Higher Education in Poland no. 0612/SBAD/3628).

## Conflict of interest

The authors declare that there are no known competing financial interests or personal relationships that could have influenced the work described in this paper.

## Authors' contributions

Krzysztof Magnucki: conceptualization, investigation, formal analysis, writing – original draft preparation, Paweł Jasion: investigation, methodology, visualization, writing – review and editing. All authors reviewed and approved the final manuscript.

## References

1. Trahair N.S., Bradford M.A., Nethercot D.A., Gardner L., *The Behaviour and Design of Steel Structures to EC3*, 4 ed., Taylor & Francis Group, London, 2008.

2. Basaglia C., Camotim D., Silvestre N., Global buckling analysis of plane and space thin-walled frames in the context of GBT, *Thin-Walled Structures*, **46**(1): 79–101, 2008, https://doi.org/10.1016/j.tws.2007.07.007.

3. Basaglia C., Camotim D., Silvestre N., GBT-based local, distortional and global buckling analysis of thin-walled steel frames, *Thin-Walled Structures*, **47**(11): 1246–1264, 2009, https://doi.org/10.1016/j.tws.2009.04.003.

4. Camotim D., Basaglia C., Silvestre N., GBT buckling analysis of thin-walled steel frames: A state-of-the-art report, *Thin-Walled Structures*, **48**(10–11): 726–743, 2010, https://doi.org/10.1016/j.tws.2009.12.003.

5. Magnucka-Blandzi E., Magnucki K., Buckling and optimal design of cold-formed thin-walled beams: Review of selected problems, *Thin-Walled Structures*, **49**(5): 554–561, 2011, https://doi.org/10.1016/j.tws.2010.09.011.

6. Magnucki K., Milecki S., Elastic buckling of a thin-walled rectangular frame under in-plane compression, *Thin-Walled Structures*, **116**: 326–332, 2017, https://doi.org/10.1016/j.tws.2017.03.007.

7. Nagy Z., Kelemen A., Nedelcu M., The influence on portal frame buckling of different cladding systems – A comparative numerical study considering stressed skin effect, *Thin-Walled Structures*, **182**(Part B): 110310, 2023, https://doi.org/10.1016/j.tws.2022.110310.

8. Krystosik P., On the columns buckling length of unbraced steel frames with semi-rigid joints, *Archives of Civil Engineering*, **67**(1): 539–556, 2021, https://doi.org/10.24425/ace.2021.136488.

9. Zhang M., Xie X., Gao X., Pan Y., Parke G., Study on failure criterion of thin-walled steel frame structures based on the ESED parameter, *Thin-Walled Structures*, **161**: 107357, 2021, https://doi.org/10.1016/j.tws.2020.107357.

10. Liu Y.Z., Yang Y.B., C X.H., Guo D.Z., Lateral-distortional buckling of frames composed of non-aligned I-members by a simple distortional beam element considering angling effect, *Thin-Walled Structures*, **202**: 112146, 2024, https://doi.org/10.1016/j.tws.2024.112146.

11. Giżejowski M.A., Szczerba R.B., Stachura Z., Gajewski M.D., Buckling resistance of quasi-straight H-section beam-columns under unequal end moments, *Archives of Civil Engineering*, **67**(1): 323–349, 2021, https://doi.org/10.24425/ace.2021.136476.

12. Zhou Y., Ning S., Huang D., Li Y., Refined plastic hinge method for steel frames with local–global interactive buckling, *Thin-Walled Structures*, **181**: 110013, 2022, https://doi.org/10.1016/j.tws.2022.110013.

13. Wen Y., He W.J., Zhan W., Li B.H., Full beam formulation for the lateral torsional buckling analysis of elastic frames by considering the structural detail of beam-to-column joint, *Thin-Walled Structures*, **183**: 110414, 2023, https://doi.org/10.1016/j.tws.2022.110414.

14. Yang Y., Hui Y., Li P., Yang Y., Huang Q., Giunta G., Belouettar S., Hu H., Global/local buckling analysis of thin-walled I-section beams via hierarchical one-dimensional finite elements, *Engineering Structures*, **280**: 115705, 2023, https://doi.org/10.1016/j.engstruct.2023.115705.

15. Xiang Y., Zhou X., Shi Y., Zhou J., Ke K., Deng F., Study on the seismic performance of cold-formed thin-walled steel frame with K-shaped braced shear panel, *Thin-Walled Structures* **184**: 110449, 2023, https://doi.org/10.1016/j.tws.2022.110449.

16. Jůza J., Jandera M., Křemen T., Experimental investigation on the square and rectangular hollow section stainless steel portal frames, *Thin-Walled Structures*, **189**: 110897, 2023, https://doi.org/10.1016/j.tws.2023.110897.

17. MAGNUCKI K., Bending of a five-layered composite beam with consideration of two analytical models, *Archive of Mechanical Engineering*, **71**(1): 27–46, 2024, https://doi.org/10.24425/ame.2024.149188.

18. MAGNUCKI K., Free flexural vibrations of standard wide-flange H-beams with consideration of the shear effect, *Rail Vehicles/Pojazdy Szynowe*, (1–2): 46–50, 2024, https://doi.org/10.53502/RAIL-189244.

*Received August 21, 2025; revised December 18, 2025; accepted December 22, 2025; available online January 14, 2026; version of record June 8, 2026; published issue XXXX.*